Chemical Engineering Science 120 (2014) 117–129

Contents lists available at ScienceDirect

Chemical Engineering Science

journal homepage: www.elsevier.com/locate/ces

Numerical simulations of lateral solid mixing in gas-fluidized beds

Oyebanjo Oke [a], Paola Lettieri [a], Piero Salatino [b], Roberto Solimene [c], Luca Mazzei [a,*]

[a] Department of Chemical Engineering, University College London, WC1E 7JE, London, UK
[b] Dipartimento di Ingegneria Chimica, dei Materiali e della Produzione Industriale, Università degli Studi di Napoli Federico II, P.le Tecchio, Napoli, Italy
[c] Istituto di Ricerche sulla Combustione, Consiglio Nazionale delle Ricerche, P.le Tecchio, Napoli, Italy

HIGHLIGHTS

- We model lateral solid mixing in fluidized beds using the Eulerian modeling approach.
- We quantify mixing by means of a lateral dispersion coefficient.
- We investigate how design parameters and operational conditions affect the coefficient.
- We examine the influence of frictional stress models on the numerical results.

ARTICLE INFO

Article history:
Received 20 June 2014
Received in revised form
19 August 2014
Accepted 23 August 2014
Available online 10 September 2014

Keywords:
Multiphase flows
Fluidization
CFD
Lateral solid mixing
Dispersion coefficient
Frictional solid stress

ABSTRACT

We investigated the influence of design parameters and operational conditions on lateral solid mixing in fluidized beds adopting the Eulerian-Eulerian modeling approach. To quantify the rate at which solids mix laterally, we used a lateral dispersion coefficient (D_{sr}). Following the usual approach employed in the literature, we defined D_{sr} by means of an equation analogous to Fick's law of diffusion. To estimate D_{sr}, we fitted the void-free solid volume fraction radial profiles obtained numerically with those obtained analytically by solving Fick's law. The profiles match very well. Our results show that D_{sr} increases as superficial gas velocity and bed height increase; furthermore, it initially increases with bed width, but then remains approximately constant. The values of D_{sr} obtained numerically are larger than the experimental ones, within the same order of magnitude. The overestimation has a twofold explanation. On one side, it reflects the different dimensionality of simulations (2D) as compared with real fluidized beds (3D), which affects the degrees of freedom of particle lateral motion. On the other, it is related to the way frictional solid stress was modeled: we employed the kinetic theory of granular flow model for the frictional solid pressure and the model of Schaeffer (1987) for the frictional solid viscosity. To investigate how sensitive the numerical results are on the constitutive model adopted for the frictional stress, we ran the simulations again using different frictional models and changing the solid volume fraction at which the bed is assumed to enter the frictional flow regime (ϕ_{min}). We observed that D_{sr} is quite sensitive to the latter. This is because this threshold value influences the size and behavior of the bubbles in the bed. We obtained the best predictions for $\phi_{min} = 0.50$. The results show that accurate prediction of lateral solid dispersion depends on adequate understanding of the frictional flow regime, and accurate modeling of the frictional stress which characterizes it.

1. Introduction

Fluidization is an operation in which a bed of granular material is made to behave like a fluid. This occurs when there is an upward flow of fluid through the granular material that makes the drag force exerted on it counterbalance its effective weight. This operation has been a winning technology, having applications in many industrial processes, such as coal combustion, biomass gasification, waste to energy conversion, sulfide roasting and food processing. Many of these processes rely on intense mixing in the fluidized bed, which creates intimate contact between the fluid and solid phases, intensifying heat and mass transfer.

To design and operate large-scale fluidized beds safely and efficiently, one needs to achieve good solid mixing in both lateral (horizontal) and axial (vertical) directions. For instance, one sees the importance of lateral solid mixing in fluidized bed combustors; in the latter, the rate at which solid fuel mixes laterally strongly influences the plant performance, affecting combustion efficiency, allocation of heat release and formation of emissions (Gómez-Barea and Leckner, 2010). It is therefore crucial to ensure that fuel

* Corresponding author: Tel: +44 (0)20 7679 4328; fax: +44 (0)20 7383 2348.
E-mail address: l.mazzei@ucl.ac.uk (L. Mazzei).

http://dx.doi.org/10.1016/j.ces.2014.08.049

spread homogeneously and rapidly over the whole cross-section of the bed. One way of achieving this is to feed the fuel at multiple entry points with the aid of a spreader; however, each added feed point increases the installation costs, and consequently one should aim to minimize their number. The knowledge of how fuel mixes laterally in a combustor is also crucial for minimizing excess air; the latter causes energy loss in the system and thus increases cost. Therefore, knowing how fuel mixes laterally is essential for improving the design of fluidized bed combustors. Efficient operation of the latter, naturally, also depends on how well mixing is achieved vertically.

To quantify the rate at which solids mix in fluidized beds, researchers often resort to axial and lateral dispersion coefficients; these, as we shall see in this study, are *effective* diffusivities relating to the times that solids take to spread axially and laterally over a given distance in the bed. Recently, researchers have made considerable efforts to analyze lateral dispersion coefficients more closely; this is because earlier studies (May 1956; Lewis et al., 1962; Avidan and Yerushalmi, 1985) concentrated mainly on axial dispersion. Notwithstanding, lateral dispersion is essential in the design and operation of large-scale beds, the coefficient quantifying it being a key input parameter in many models for fluidized bed reactors.

Despite the importance of lateral solid mixing, there is a dearth of research on this subject, the available works focusing mainly on the experimental methods of estimating lateral dispersion coefficients. Kashyap and Gidaspow (2011) summarized these methods as *saline* (Rhodes et al., 1991), *ferromagnetic* (Avidan and Yerushalmi, 1985), *thermal* (Borodulya and Epanov, 1982), *radioactive* (Mostoufi and Chaouki, 2001), *carbon* (Winaya et al., 2007) and *phosphorescent* (Du et al., 2002) tracing methods. These experimental approaches have their limitations: in thermal tracking techniques heat is transferred to the fluid phase and walls, making it difficult to interpret the results; in radioactive tracking methods safety of equipment and personnel are of great concern; in phosphorescence tracking methods most successful applications usually take place in dilute fluidized beds. For all solid tracer techniques, the common limitation is that repeatable results are only guaranteed if numerous runs of experiments are carried out, a condition that may not be practicable in real experiments. In addition, experiments with solid tracers are difficult to perform because of lack of continuous sampling and presence of residual tracer. Despite these experimental investigations, the understanding of how design parameters and operating conditions affect lateral dispersion coefficients is still limited, because the mechanisms governing solid mixing are complex.

In recent times, computational fluid dynamics (CFD) simulation provides a powerful tool, complementary to experiments, to investigate the dynamics of fluidized beds (Gidaspow, 1994; Mazzei and Lettieri, 2008, Mazzei et al., 2010; Mazzei, 2011, 2013). The model equations are based on first principles: the balance equation for mass, momentum and energy. Two modeling approaches are usually adopted: the Eulerian-Eulerian and the Eulerian-Lagrangian (Lettieri and Mazzei, 2009). In the former, averaged equations describe the fluid and the solid as interpenetrating continua. In the latter, conversely, one tracks the motion of each particle and solves the average equations of motion only for the continuous phase. The first approach offers the advantage of being relatively less computationally demanding, providing information of direct interest in applications (for example, average velocity fields and volume fractions). The other approach is useful in providing enormous details of the fluid bed dynamics, and is an approach of choice for researchers who are interested in gaining deeper insight into the dynamics of granular media. The CFD modeling approach has proven to be effective in studying the dynamics of fluidized beds (Coroneo et al., 2011; Tagliaferri et al., 2013), offering distinct advantages: an accurate CFD model can considerably aid in the design of the bed, saves time and improves the confidence of plant scale-up.

Despite these advantages, studies on lateral solid dispersion in fluidized beds using numerical approaches are still scanty. This has hindered the advancement of knowledge on how various design parameters and operating conditions affect fluid bed processes. To the best of our knowledge, numerical works on lateral solid dispersion in fluidized beds have only been carried out by Liu and Chen (2010) and Farzaneh et al., (2011). Liu and Chen (2010) employed the Eulerian-Eulerian approach to estimate the lateral dispersion coefficients using a micro and a macro method. The latter fits the transient particle concentration profile obtained numerically with the solution of a Fickian-type diffusion equation, while the former generates statistics of particles by using a random walk approach. Farzaneh et al., (2011), on the other hand, adopted a multi-grid Eulerian-Lagrangian approach.

In this work, we aimed to use and test a Eulerian-Eulerian model that one could employ to estimate lateral solid dispersion coefficients (we did not intend, nevertheless, to derive a numerical correlation for them). The model describes both solid and fluid phases as interpenetrating continua. It consists of the continuity equations and linear momentum balance equations written for each phase. These equations are valid for any physical and chemical system, and therefore this approach does not introduce any assumption in the model, except for the constitutive equations needed to render the equations mathematically closed. We follow an approach similar to that proposed by Brotz (1956). He used two solids of equal physical properties, but differing in color. The solids were separated by a vertical partition plate which divided the bed into two equal parts. He fluidized the bed for a certain time and then removed the partition; by measuring the rate at which the two solids mix, he estimated the lateral dispersion coefficient. With Brotz, we defined two solid phases, Solid-1 and Solid-2, with equal physical properties, differing only in the names assigned to them in the computational code. We then placed Solid-1 on the left and Solid-2 on the right of a removable partition. We fluidized the bed with air at ambient temperature, allowing it to reach pseudo-stationary conditions, and then removed the partition. From the radial concentration of the Solid-1 phase, we estimated the lateral solid dispersion coefficient at the assigned operating conditions. Before advancing further, let us briefly discuss how D_{sr} is defined in this work.

2. Lateral dispersion coefficient – definition and estimation

Sometimes one might be interested in *estimating* how fast particles mix in a fluid bed at given operating conditions, without wanting to solve complex and numerically expensive models. One way of doing this is resorting to axial and lateral *dispersion coefficients*; these, as said, are *effective* diffusivities relating to the time that solids take to spread axially and laterally over a given distance in the bed. We are going to focus on the lateral dispersion coefficient; therefore, before going any further, let us clarify how the latter is defined. Most researchers (Brotz, 1956; Borodulya and Epanov, 1982; Shi and Fan, 1984; Liu and Chen, 2010) define it through an equation analogous to Fick's law of molecular diffusion, writing:

$$\partial_t C = D_{sr}\partial^2_{xx} C \tag{1}$$

where C represents the void-free solids concentration and D_{sr} represents the lateral dispersion coefficient. This equation, as just said, should be regarded as a *definition* of such coefficient. Let us briefly comment on the applicability of Eq. (1) to the present investigation. One might wonder how the diffusion equation above

can be relevant to the study of lateral solid mixing in fluidized beds. Lacey (1954) proposed a diffusion-like mechanism for solid mixing, arguing that particles spread through a surface in a manner similar to ordinary molecular or thermal diffusion. Each particle has equal chance of moving to either side of the surface, closely resembling the motion of molecules of a gas. Indeed, experimental data obtained by Carstensen and Patel (1977) revealed that mixing of binary particles can be well characterized by Eq. (1) as long as the mean diameters of the particles are identical, the coefficient D_{sr} appearing in the equation lumping together the effects of various mechanisms responsible for solid mixing such as: wake transport, emulsion drifting, bubble coalescence and break-up. For shallow beds, particle ejection/fall-back in the freeboard upon bubble bursting at the bed surface may also be relevant.

Take a 2D bed (we consider two dimensions to simplify the description, but similar considerations hold in three dimensions) where the concentration of solids depends in general on both spatial coordinates, so that $c = c(x, y, t)$, with x and y denoting the horizontal and vertical coordinates, respectively. The concentration in Eq. (1) is averaged over the vertical direction, and hence is a function of the x coordinate only, so that $C = C(x, t)$. For a given system, by matching the actual concentration function $C_e(x, t)$, which one can determine either experimentally or numerically, with the analytical solution of Eq. (1), one can find the lateral dispersion coefficient. We should bear in mind that, unlike molecular diffusion coefficients, D_{sr} is not just a function of the particle properties, but depends on the system geometry and on the operating conditions; this should be apparent from its definition.

Let us be more specific. Often, to determine the lateral dispersion coefficient, one considers a bed divided into two equal compartments; the particles occupying the compartments differ solely in color (having in particular same size and density). For instance, one can have black particles in the left compartment and white particles in the other. The functions $c(x, y, t)$ and $C(x, t)$ represent the concentration of just one kind of particles, say the black ones, which are regarded as tracer particles. Hence, the initial conditions characterizing this particular setup are:

$$t = 0: \quad C = \overline{C} \quad for \quad 0 \le x < \frac{L}{2} \quad and \; C = 0 \; for \; \frac{L}{2} < x \le L \tag{2}$$

The boundary conditions that one needs to assign to solve Eq. (1) are:

$$x = 0, \quad x = L: \quad \partial_x C = 0 \tag{3}$$

In the real experiment (which may be numerical) the two compartments, as reported above, are separated by a removable wall. At time $t = 0$, one fluidizes the system, waiting for the latter to reach pseudo-stationary conditions. Then one removes the partition, letting the black and white particles spread through the bed. The void-free concentration of black particles, which one in theory could measure (or calculate numerically), is $c(x, y, t)$. One can then divide the bed in a given number of vertical layers and calculate the mean value of C_e in each layer using the relation:

$$C_e(x, t) \equiv \frac{1}{V_L} \int_{V_L} c(x, y, t) dV \tag{4}$$

where V_L denotes the volume of each vertical layer. The next step is solving Eq. (1), using the conditions in Eqs. (2) and (3). For this simple system an analytical solution is available (Hirama et al., 1975):

$$C(x,\ t; D_{sr}) = \frac{1}{2} + \frac{2}{\pi} \sum_{a=1}^{\infty} \frac{1}{a} sin\left(\frac{a\pi}{2}\right) cos\left(a\pi \frac{x}{L}\right) exp\left(-a^2\pi^2 \frac{t}{L^2/D_{sr}}\right) \tag{5}$$

Here we have reported explicitly the dependence of the analytical solution on the parameter D_{sr}. Then, to estimate D_{sr} we simply match the profiles $C_e(x, t)$ and $C(x,\ t; D_{sr})$. To do this, we define:

$$G \equiv [C(x,\ t; D_{sr}) - C_e(x, t)]^2 \tag{6}$$

The task of determining D_{sr} then reduces to finding the value of D_{sr} that minimizes G in Eq. (6). This value gives the lateral dispersion coefficient for the system under investigation.

By repeating this procedure for many geometries and operating conditions, one can obtain a correlation of the form written in Eq. (7), which others can then use to estimate D_{sr}; this reduces the need for solving complex models or conducting experiments each time one is interested in estimating D_{sr}.

$$\frac{D_{sr}}{(u - u_{mf}) h_{mf}} = f\left(\frac{\rho_f (u - u_{mf})\, d_p}{\mu_f}, \frac{h_{mf}}{d_p}, \frac{\rho_p - \rho_f}{\rho_f}, \frac{L}{d_p}\right) \tag{7}$$

Here u is the superficial gas velocity, u_{mf} the minimum fluidization velocity, h_{mf} the bed height at minimum fluidization, ρ_p the particle density, ρ_f the fluid density, μ_f the fluid viscosity and L the bed width.

As said, one can use the lateral dispersion coefficient D_{sr} to roughly estimate the time τ that solids take to spread laterally over a distance L in the bed. To demonstrate this, we note that:

$$\frac{\partial C}{\partial t} \sim \frac{\overline{C}}{\tau} \quad ; \quad \frac{\partial C}{\partial x} \sim \frac{\overline{C}}{L} \quad ; \quad \frac{\partial}{\partial x}\left(\frac{\partial C}{\partial x}\right) \sim \frac{\overline{C}/L}{L} = \frac{\overline{C}}{L^2}$$

where $\overline{C}$ represents the concentration scale (whose value does not affect τ, because Eq. (1) is linear in the concentration). Eq. (1) thus yields:

$$\tau \sim \frac{L^2}{D_{sr}} \tag{8}$$

So, if one knows the value of D_{sr} for a given design and set of operating conditions, one can estimate the time τ required for the solids to spread laterally over the length L in the bed.

We would like to emphasize that the parameter D_{sr} in Eq. (1) is different from the coefficient appearing in the original Fick's law. In the latter the parameter is molecular diffusivity, which is constant for a solute in a given solvent. Fick's law relates only to the diffusion of molecules generated by their random motion. The lateral dispersion coefficient, conversely, is affected by various competing mechanisms. These, as experimental evidence reveals, include bubble break-up at the upper bed surface and subsequent ejection of particles into the freeboard, wake transport and drifting of emulsion owing to the passage of bubbles. Hence, the lateral dispersion coefficient is affected by several variables, among which we find bubble size and velocity, particle size and density as well as fluid density and viscosity. Shi and Fan (1984) reported that gross particle circulation also affects lateral mixing, this circulation in turn depending on bed height and superficial gas velocity. Determining D_{sr} is therefore quite challenging.

Another clarification is in order. As said, when calculating lateral dispersion coefficients, we operated in terms of concentrations averaged along the vertical direction of the bed, considering the function $C(x, t)$, defined through Eq. (4), in place of the function $c(x, y, t)$. In doing so, we lost information about vertical variations in concentration, which we expect to be present; these variations, nevertheless, are accounted for, inasmuch as they affect the value of $C(x, t)$ and in turn that of D_{sr}. We had to operate in terms of vertically averaged concentrations, for we decided to define D_{sr} through Eq. (1), which is one-dimensional and accounts solely for variations along the horizontal space coordinate. We employed Eq. (1) to define D_{sr} because this is the relation usually used in the literature; in particular, the researchers cited in this article who measured D_{sr} experimentally – and whose results we used to validate our simulations – did adopt this definition and, as

a consequence, operated in terms of vertically averaged concentrations.

3. Multiphase fluid dynamic model

The governing equations in this work consist of balance equations for mass and linear momentum written for the fluid and the two solid phases:

Continuity equation – Fluid phase

$$\partial_t \varepsilon = -\nabla \cdot \varepsilon \boldsymbol{u_e} \tag{9}$$

Continuity equation – Solid phase i

$$\partial_t \phi_i = -\nabla \cdot \phi_i \boldsymbol{u_i} \tag{10}$$

Dynamical equation – Fluid phase

$$\partial_t (\varepsilon \rho_e \boldsymbol{u_e}) = -\nabla \cdot (\varepsilon \rho_e \boldsymbol{u_e u_e}) + \nabla \cdot \boldsymbol{S_e} - n_1 \boldsymbol{f}_1 - n_2 \boldsymbol{f}_2 + \varepsilon \rho_e \boldsymbol{g} \tag{11}$$

Dynamical equation – Solid phase i

$$\partial_t (\phi_i \rho_i \boldsymbol{u_i}) = -\nabla \cdot (\phi_i \rho_i \boldsymbol{u_i u_i}) + \nabla \cdot \boldsymbol{S_i} + n_i \boldsymbol{f_i} - n_i \boldsymbol{f_{ik}} + \phi_i \rho_i \boldsymbol{g} \tag{12}$$

Here i is a phase index, subscripts 1 and 2 identify the solid to the left and to the right of the partition, respectively (as reported in Section 2), ρ_e and ρ_i, ε and ϕ_i are the densities and volume fractions of the fluid and solid phases, respectively, while $\boldsymbol{g}$ is the gravitational acceleration. Furthermore, $\boldsymbol{u_e}$, $\boldsymbol{u_i}$, $\boldsymbol{S_e}$, $\boldsymbol{S_i}$, $\boldsymbol{f_i}$, and $\boldsymbol{f_{ik}}$ are the averaged velocities, effective stress tensors and interaction forces per unit particle exerted by the fluid and by the kth solid phase on the ith solid phase, respectively. The equations written above are unclosed; various terms need to be expressed constitutively.

3.1. Fluid-particle interaction forces

The main components of the fluid-particle interaction force are the buoyancy and drag forces. We neglect other contributions (Owoyemi et al., 2007); thus, we write $\boldsymbol{f_i} = \boldsymbol{f_i}^{s} + \boldsymbol{f_i}^{d}$. We define the buoyancy force as $n_i \boldsymbol{f_i}^{s} \equiv -\phi_i \nabla p_e$. We close the drag force using the expression of Mazzei and Lettieri (2007):

$$n_i \boldsymbol{f_i}^{d} \equiv \beta_i (\boldsymbol{u_e} - \boldsymbol{u_i}) \quad ; \quad \beta_i = \frac{3}{4} C_D(Re_i) \frac{\rho_e \| \boldsymbol{u_e} - \boldsymbol{u_i} \| \varepsilon \phi_i}{d_i} \varepsilon^{-\psi(\varepsilon, Re_i)} \tag{13}$$

$$\psi(\varepsilon,\ Re_i) \equiv -\frac{\ln \varphi(\varepsilon, Re_i)}{\ln \varepsilon} \quad ; \quad \varphi(\varepsilon, Re_i) \equiv \frac{C_D^*(\varepsilon, Re_i)}{C_D(Re_i)} \varepsilon^{2(1-n)}$$

$$C_D(Re_i) = (0.63 + 4.8 Re_i^{-(1/2)})^2 \ ; \ C_D^*(\varepsilon, Re_i^*) = (0.63 + 4.8 Re_i^{*-(1/2)})^2$$

$$Re_i \equiv \frac{\rho_e}{\mu_e} \varepsilon \| \boldsymbol{u_e} - \boldsymbol{u_i} \| d_i \quad ; \quad Re_i^*(\varepsilon, Re_i) \equiv \frac{Re_i}{\varepsilon^n};$$

$$n(Re_i^*) = \frac{4.8 + 2.4 \cdot 0.175 Re_i^{*3/4}}{1 + 0.175 Re_i^{*3/4}} \tag{14}$$

Here d_i is the particle diameter of the ith solid phase, Re_i and Re_i^* are particle Reynolds numbers, while C_D and C_D^* are drag coefficients.

3.2. Particle-particle interaction force

We assume that the interaction force $\boldsymbol{f_{ik}}$ exchanged between particles of different phases includes only a drag-like contribution. Therefore, it is proportional to the slip velocity between the phases. We used the constitutive equation developed by Syamlal (1987):

$$n_i \boldsymbol{f_{ik}} = \zeta_{ik} (\boldsymbol{u_k} - \boldsymbol{u_i});$$

$$\zeta_{ik} = \frac{3}{4}(1 + e_{ik}) \left(1 + \frac{\pi}{4} F_{ik}\right) \frac{\rho_i \rho_k \phi_i \phi_k g_{ik} (d_i + d_k)^2}{\rho_i {d_i}^3 + \rho_k {d_k}^3} \| \boldsymbol{u_k} - \boldsymbol{u_i} \| \tag{15}$$

where e_{ik} is a coefficient of restitution equal to 0.90, F_{ik} is a coefficient of friction equal to 0.15 and g_{ik} is a radial distribution function that one obtains by combining the radial distribution functions g_i and g_k of the ith and kth particle phases, respectively. Their expressions are:

$$g_i = \frac{d_i}{2} \sum_{k=1}^{2} \frac{\phi_k}{d_k} + \left[1 - \left(\frac{\phi}{\phi_{max}}\right)^{1/3}\right]^{-1} \quad ; \quad g_{ik} = \frac{d_i g_k + d_k g_i}{d_i + d_k} \tag{16}$$

Here ϕ is the overall solid volume fraction, while ϕ_{max} is the maximum value that ϕ can attain.

3.3. Effective stress

We close the effective stress tensors using the Newtonian constitutive equation:

$$\boldsymbol{S_e} = -p_e \boldsymbol{I} + 2\mu_e \boldsymbol{D_e} + \left(\kappa_e - \frac{2}{3}\mu_e\right)(\mathrm{tr}\boldsymbol{D_e})\boldsymbol{I} \quad ;$$

$$\boldsymbol{S_i} = -p_i \boldsymbol{I} + 2\mu_i \boldsymbol{D_i} + \left(\kappa_i - \frac{2}{3}\mu_i\right)(\mathrm{tr}\boldsymbol{D_i})I \tag{17}$$

where p_e, p_i, μ_e, μ_i, κ_e and κ_i are the averaged pressures, viscosities and dilatational viscosities of the fluid and particle phases, respectively; $\boldsymbol{I}$ is the identity tensor, while $\boldsymbol{D_e}$ and $\boldsymbol{D_i}$ are the rate of deformation tensors defined as:

$$\boldsymbol{D_e} \equiv \frac{1}{2}(\nabla \boldsymbol{u_e} + \nabla \boldsymbol{u_e}^T) \quad ; \quad \boldsymbol{D_i} \equiv \frac{1}{2}(\nabla \boldsymbol{u_i} + \nabla \boldsymbol{u_i}^T) \tag{18}$$

Closing the effective stress tensors therefore reduces to finding constitutive expressions for the pressure, viscosity and dilatational viscosity of each phase. The fluid is regarded as incompressible and so the fluid pressure does not need a constitutive expression. The viscosity μ_e is assumed to be constant, while the dilatational viscosity κ_e is neglected. For the solid phases, we need constitutive expressions to model all these quantities.

The solid phase can be in two flow regimes: the *viscous regime* where particles undergo transient contacts and momentum transfer is translational and collisional, and the *frictional regime*, where particles are in enduring contacts and momentum transfer is mainly frictional. In both regimes, the solid phase is modeled as a continuum; in the viscous regime it is characterized by a viscous solid pressure ${p_i}^v$, viscosity ${\mu_i}^v$ and dilatational viscosity ${\kappa_i}^v$, while in the frictional flow regime it is characterized by a frictional solid pressure ${p_i}^f$, viscosity ${\mu_i}^f$ and dilatational viscosity ${\kappa_i}^f$.

We express ${p_i}^v$ using the closure of Lun et al. (1984):

$${p_i}^v = \left[1 + 2 \sum_{k=1}^{2} \left(\frac{d_{ik}}{d_i}\right)^3 (1 + e_{ik}) \phi_k g_{ik}\right] \phi_i \rho_i \Theta_i \quad ; \quad d_{ik} \equiv \frac{d_i + d_k}{2} \tag{19}$$

Here Θ_i is the granular temperature of the ith phase. In the present study, $d_i = d_k$, e_{ii} coincides with the restitution coefficient e_i and g_{ik} reduces to g_i. For the viscosity ${\mu_i}^v$ we adopt the closure of Gidaspow (1994):

$${\mu_i}^v = \frac{10 \rho_i d_i \sqrt{\pi \Theta_i}}{96(1 + e_i) g_i} \left[1 + \frac{4}{5}(1 + e_i)\phi_i g_i\right]^2 + \frac{4}{5}{\phi_i}^2 \rho_i d_i g_i (1 + e_i) \left(\frac{\Theta_i}{\pi}\right)^{\frac{1}{2}} \tag{20}$$

For the dilatational viscosity ${\kappa_i}^v$ we use the closure of Lun et al. (1984):

$${\kappa_i}^v = \frac{4}{3}{\phi_i}^2 \rho_i d_i g_i (1 + e_i) \left(\frac{\Theta_i}{\pi}\right)^{\frac{1}{2}} \tag{21}$$

The granular temperatures are governed by balance equations for the pseudointernal energies related to the fluctuation velocities of the particles (Gidaspow, 1994; Syamlal et al., 1993). The equation reads:

$$\partial_t (\phi_i \rho_i U_i) = -\nabla \cdot (\phi_i \rho_i U_i \boldsymbol{u_i}) - \nabla \cdot \boldsymbol{q_i} + \boldsymbol{S_i} : \nabla \boldsymbol{u_i} + {G_i}^d - {S_i}^v - {S_i}^c \tag{22}$$

where ${S_i}^c$ is a sink term representing losses of pseudointernal energy caused by inelastic collisions, ${G_i}^d$ is a source term

representing the generation of particle velocity fluctuations by fluctuating fluid-particle forces, while S_i^{ν} is a sink term representing dampening of particle velocity fluctuations caused by viscous resistance to particle motion. The pseudointernal energy per unit particle mass is $U_i = 3\Theta_i/2$, and $\boldsymbol{q_i}$ is the pseudothermal heat flux. For the closures of $\boldsymbol{q_i}$, G_i^{d}, S_i^{ν} and S_i^{c} we refer to Gidaspow (1994).

In the frictional flow regime, as reported earlier, particles interact largely through frictional enduring contacts. These are not accounted for by the kinetic theory of granular flow. Therefore, to model the flow properties in this regime, one needs to adopt the theories of plasticity and soil mechanics. Shaeffer (1987) developed a model that relates μ_i^f to p_i^f based on the principles of soil mechanics. The model reads:

$$\mu_i^f = \frac{p_i^f \sin\varphi}{2\sqrt{I_2}} \tag{23}$$

where φ is the angle of internal friction and I_2 is the second invariant of the deviatoric stress tensor. The frictional solid pressure is often modeled by means of arbitrary functions that have no theoretical basis but correctly describe qualitatively how dense granular media behave (Syamlal et al., 1993). The prime feature that must be captured is that such materials cannot reach compactions that are unphysically high. A closure for the frictional solid pressure that some modelers use is:

$$p_i^f = \phi_i p^* \quad \text{where } p^* \equiv 10^A(\phi - \phi_{min})^B \tag{24}$$

where ϕ_{min} is the frictional packing limit, and A and B are coefficients having typical values of 25 and 10, respectively. This equation is extremely sensitive to the deviation of ϕ from ϕ_{min} and this could lead to big pressure fluctuations and violent numerical instabilities (Schaeffer, 1987). Eq. (24) is often employed with radial distribution functions that are bounded and so do not diverge positively when ϕ approaches ϕ_{max}. For instance, the model of Syamlal et al. (1993), used in the CFD code MFIX, adopts the expression of Lebowitz (1964):

$$g_i = \left(1 + \frac{3d_i}{2\varepsilon}\sum_{k=1}^{2}\frac{\phi_k}{d_k}\right) \tag{25}$$

where, as opposed to Eq. (16), ϕ_{max} does not feature. As in Eq. (16) g_i diverges when ϕ approaches ϕ_{max}, the viscous solid pressure already prevents the mixture from overpacking; therefore, one can use the same equation used to model the viscous solid pressure, that is, Eq. (19), to model also the total solid pressure in the frictional regime (instead of summing to the viscous solid pressure an additional contribution modeled by means of an arbitrary divergent function, qualitatively sound but theoretically unfounded).

These considerations induced us to employ the so-called KTGF-based model, a frictional model partly based on the kinetic theory of granular flows (KTGF) which accounts only for the frictional viscosity μ_i^f neglecting the frictional solid pressure p_i^f and the frictional dilatational viscosity κ_i^f. When ϕ exceeds ϕ_f, the model keeps on using the viscous closure for the solid pressure, Eq. (19), but increases the solid viscosity by adding to the viscous contribution, Eq. (20), the frictional one given by Eq. (23). As a consequence, the solid viscosity becomes:

$$\mu_i = \mu_i^f + \mu_i^{\nu} \tag{26}$$

In Eq. (23) the pressure used in the calculation is the viscous solid pressure (which, as said, coincides with the total solid pressure, since the frictional solid pressure is not considered).

3.4. Boundary and initial conditions

The computational grid (uniform, with square cells of 5 mm side) is two dimensional; hence the front and back wall effects are neglected. On the left, right and middle walls, no-slip boundary conditions apply. At the bottom of the bed, a uniform inlet fluid velocity u is specified. The fluid is ambient air. At the upper boundary, the pressure is set to 10^5 *Pa*. On all the boundaries, the solid mass fluxes are set to zero.

Initially, the bed is fixed and consists of two equal and adjacent compartments partitioned by a removable wall. Each compartment consists of solids having the same size and density. The voidage is set to 0.4 everywhere in the bed. We fluidize the solids in each compartment with the same superficial gas velocity for about three seconds until they reach stable fluidization, and then we remove the partition. To obtain the horizontal solid volume fraction profiles in the bed, we divide the bed into twenty equal vertical layers evenly distributed over the horizontal direction and

Table 1
Simulation parameters for Powder 1.

Parameters	Value
Vessel height	0.35 m
Bed width	0.20–1.00 m
Superficial gas velocity	0.87–1.17 m/s
Particle diameter	491 μm
Particle density	2620 kg/m^3
Minimum fluidization velocity	0.20 m/s
Bed height	0.05–0.11 m
Computational cell	0.005 m
Time-step	0.001 s

Table 3
Simulation parameters for Powder 2.

Parameters	Value
Vessel height	0.60 m
Bed width	0.90 m
Superficial gas velocity	0.45–0.75 m/s
Particle diameter	595 μm
Particle density	1400 kg/m^3
Minimum fluidization velocity	0.25 m/s
Bed height	0.17–0.23 m
Computational cell	0.005 m
Time-step	0.001 s

Table 2
Summary of simulation cases.

Cases	Frictional Pressure Model		Frictional Viscosity Model		Frictional Packing Limit	
	KTGF	J & J	Schaffer	J & J	0.50	0.61
1	X		X			X
2	X		X		X	
3	X			X		X
4	X			X	X	
5		X		X	X	

we compute the void-free solid volume fraction in each layer following the procedure reported in Section 2.

4. Results

We considered two sets of powders: Powder 1 was used by Shi and Fan (1984) in their experimental study of lateral mixing of solids in batch fluidized beds, and Powder 2 was investigated by Mori and Nakamura (1965). The parameters used to simulate these powders, in particular the geometry and the bed height, are chosen to replicate the experimental work of these authors. We report in Table 1 the parameters employed in the simulations of Powder 1; those for Powder 2 are reported in Table 3.

As said earlier, we fluidized the bed, divided it into two equal parts by a removable partition, for a certain period, allowing them to reach pseudo-stationary conditions, and then removed the partition. We ran preliminary simulations, removing the partition after three and five seconds, and comparing the void-free concentration profiles obtained in the two cases. We observed that there was no significant difference between the two; consequently, in subsequent simulations, we removed the partition after three seconds.

4.1. Effect of superficial gas velocity

From the solid volume fraction profiles obtained numerically, we calculated the void-free mass fraction $\hat{\phi}_i$ of solid phase i in each layer:

$$\hat{\phi}_i \equiv \frac{\phi_i}{\phi_1+\phi_2} \tag{27}$$

We ran the simulations at various superficial gas velocities (starting from 0.87 m/s, which is the minimum velocity investigated experimentally by Shi and Fan, 1984, up to 1.17 m/s, with increments of 0.10 m/s), keeping the minimum fluidization bed height at 5.23 cm (which is the maximum bed height at minimum fluidization conditions investigated by Shi and Fan, 1984) and the bed width at 0.6 m (which is the single bed width investigated by Shi and Fan, 1984). We fitted the void-free mass fraction profiles obtained from our simulations with those obtained from Eq. (1) using the least square regression method, as reported in Section 2. In Fig. 1 we report the profiles of void-free mass fraction obtained from Eq. (1) and those obtained numerically at $t=5.0$ s. Similar profiles are found at other times, but we have chosen 5.0 s as representative time. We obtained a reasonable fit, as Fig. 1 shows. Fig. 2A reports the snapshots of particle concentrations obtained from the simulations at a superficial gas velocity of 0.87 m/s (4.35 times u_{mf}). The figure shows how particles placed at the left of the removable partition spread to the right. We observe from Fig. 2A that the spread of the particles proceeds in a manner similar to what one would observe in, for instance, the molecular diffusion of ink in water; even though in this case the spread of particles is induced primarily by bubbles. This diffusion-like spread of particles explains why we obtained a reasonable fit between our numerical results and those obtained from Eq. (1). The snapshots showing the contours of particle concentrations at superficial gas velocity of 1.17 m/s (5.85 times u_{mf}) are reported in Fig. 2B. It is interesting to observe that the contours of solid volume fraction shown in this figure are partly different from those in Fig. 2A, even though the snapshots were taken at the same computational times. In Fig. 2B we observe streams of particles transported into the freeboard in a region close to the bed surface. This is caused by the burst of bubbles and subsequent ejection of their solid content into the freeboard. As reported by Davidson and Harrison (1971), particles are carried up through the bed in the bubble wakes and, when bubbles burst, part of them spreads over the surface of the bed. This kind of solid transport is essentially absent in Fig. 2A. This additional mechanism, observed when the superficial gas velocity is larger, contributes to the higher value of D_{sr} obtained at this velocity, as reported in Fig. 3.

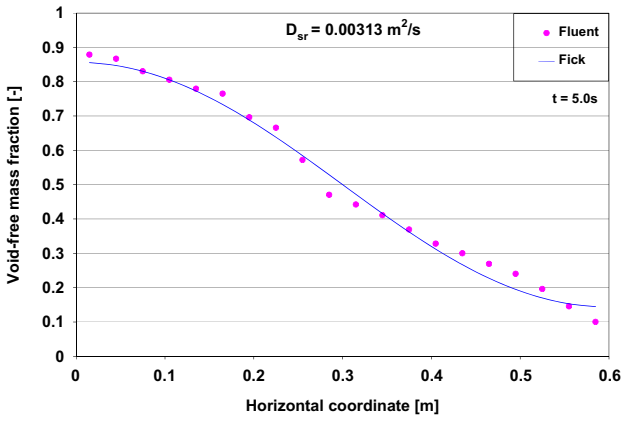

Fig. 1. Solid 1 void-free vertically averaged mass fraction horizontal profiles for a superficial fluid velocity of 0.87 m/s. The minimum fluidization bed height is 5.23 cm, while the bed width is 0.60 m. The 'Fick' profile is that obtained from the analytical solution of the Fick's law, while the 'Fluent' profile is that obtained numerically.

In Fig. 3 we plot D_{sr} against the superficial gas velocity, comparing our simulation results with those obtained from empirical correlations available in the literature. We observe that the value of the dispersion coefficient increases as the superficial gas velocity increases. This is expected, because an increase in velocity induces more vigorous mixing in the bed, rendering solid circulation more intense and enhancing lateral solid transport. As said, at higher superficial gas velocities an additional mechanism affects lateral mixing; this is the solid transport across the bed surface caused by bubble eruption. These observations were also reported by Kunii and Levenspiel (1989). Fig. 3 also shows that the numerical values of the dispersion coefficient have the same order of magnitude as those given by the empirical correlations, but in all cases overestimate the latter. The reason for this needs to be investigated.

4.2. Effect of bed height

We investigated the effect of bed height on lateral dispersion coefficients. To do this, we ran simulations at different minimum fluidization bed heights (spanning the range between 5.23 cm and 11.23 cm), fixing the superficial gas velocity at 1.07 m/s (5.35 times u_{mf}; an intermediate value in the velocity range considered in Section 4.1) and the bed width at 0.6 m. Following the same procedure outlined above, we obtained the void-free horizontal mass fraction profiles in the bed. We report in Fig. 4 the profiles when the bed height is 7.23 cm. The numerical profile fits reasonably well the analytical one obtained from Eq. (1).

As shown in Fig. 5, we observe an increase in dispersion coefficient as the bed height is increased. This is because as the bed height increases, bubbles grow in size causing more recirculation and more particles to be drawn into their wakes. As bubbles erupt at the bed surface, they eject more particles into the freeboard, enhancing the lateral transport of solids. These effects are observed in the snapshots of solid volume fraction reported in Fig. 6 for different bed heights at $t=5.0$ s. As the bed height increases, the size of bubbles increases, implying that greater volume of emulsion can be driven aside. This leads to more intense mixing, and hence increases solid lateral transport. We also compared the simulation results with empirical correlations available in the literature, as shown in Fig. 5. The values of dispersion coefficients obtained from the simulations

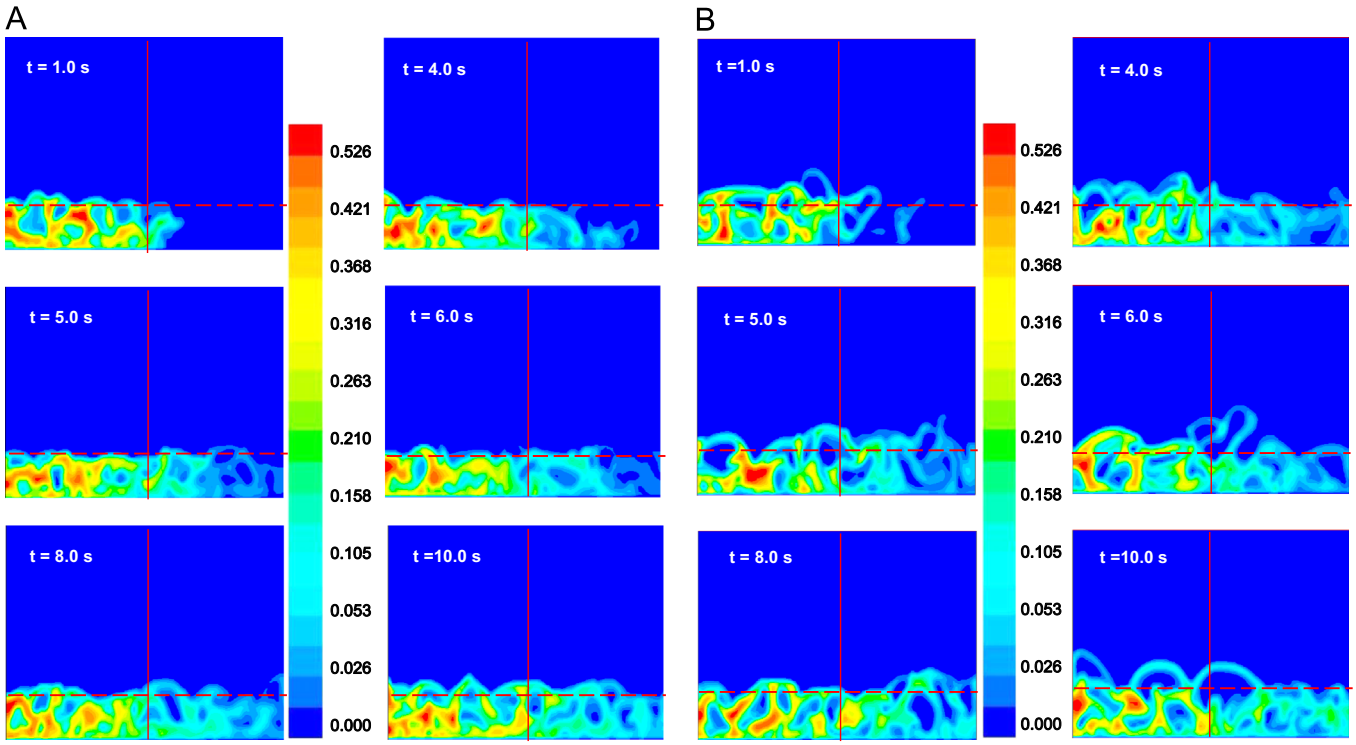

Fig. 2. Solid 1 volume fraction profiles at different times. (A) Superficial fluid velocity of 0.87 m/s. (B) Superficial fluid velocity of 1.17 m/s. The minimum fluidization bed height is 5.23 cm, while the bed width is 0.60 m. The horizontal dashed line indicates where the bed ends and the freeboard begins.

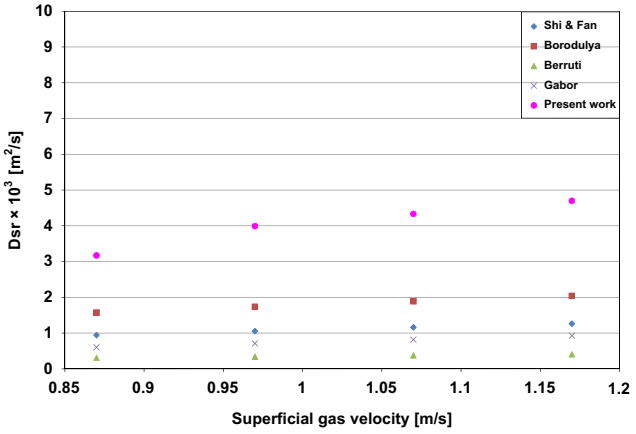

Fig. 3. Dispersion coefficient values at different superficial fluid velocities. The minimum fluidization bed height is 5.23 cm, while the bed width is 0.60 m. The values are compared with those obtained from empirical correlations in the literature.

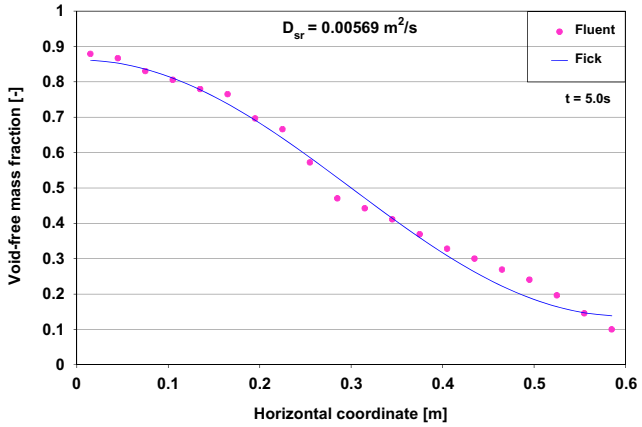

Fig. 4. Solid 1 void-free vertically averaged mass fraction horizontal profiles for a minimum fluidization bed height of 7.23 cm. The superficial fluid velocity is 1.07 m/s, while the bed width is 0.60 m. The 'Fick' profile is that obtained from the analytical solution of the Fick's law, while the 'Fluent' profile is that obtained numerically.

have the same order of magnitude as those given by the empirical correlations; again, however, the numerical results overestimate the empirical ones.

4.3. *Effect of bed width*

Most researchers investigating lateral solid dispersion in fluidized beds often neglect the influence of bed width. For instance, Shi and Fan (1984) in their experimental work on lateral solid mixing in batch gas-fluidized beds summarized the mechanisms governing lateral solid mixing as: *bubble movement through the bed, bubble burst at the surface*, and *gross particle circulation in the bed*. In summarizing the parameters on which these mechanisms depend, they did not include bed width. Several other authors (Berruti et al., 1986; Bellgardt et al., 1987; Salam et al., 1987; Xiang et al., 1987; Winaya et al., 2007) who have developed empirical correlations for lateral dispersion coefficients also ignore bed width as a parameter that might affect it. We believe that bed geometry should influence lateral mixing, and hence the coefficient quantifying it, D_{sr}. This is because bed geometry plays a crucial role in gross particle circulation, which is an important mechanism responsible for lateral solid mixing. To investigate the influence of bed width on lateral solid dispersion, we considered beds of different widths, ranging from 0.2 to 1.0 m (values smaller and larger than that used by Shi and Fan, 1984, which we employed in Sections 4.1 and 4.2). We fluidized these beds, maintaining the superficial gas velocity at 1.07 m/s and the minimum fluidization bed height at 5.23 cm. We then determined the lateral dispersion coefficient at each value of bed width, using the approach described previously. In Fig. 7, we report the values of the dispersion coefficient at different bed widths. The figure shows that the coefficient increases rapidly as the bed width increases from 0.2 to 0.4 m, afterwards increases slowly and finally

becomes approximately constant. To explain this trend, let us briefly report on the observation by Pallarès et al. (2007) regarding the mechanisms of lateral solid mixing. They reported that lateral solid mixing is due to horizontally aligned vertical vortices, rotating in alternate directions (these vortices are referred to as mixing cells). In these mixing cells, the following mechanisms for solid mixing take place: *bubble wake mixing*, *drifting aside of emulsion* and *bubble eruption at the bed surface*. The net lateral solid transport in the bed results from the exchange of solids in the mixing cells and is determined by the integral length scale of macroscopic solids circulation patterns. It is likely that the integral length scale of solids circulation be constrained by bed width for comparatively narrow beds. For wide beds the integral length scale of solids circulation, hence lateral solid transport, should rather be dictated by bed height.

5. Discussion

It is clear from the results presented above that the values of D_{sr} obtained from our simulations are larger than those predicted by empirical correlations, albeit the order of magnitude of the coefficient is correctly captured. We believe that this overestimation has two main causes. The first relates to how the frictional stress of the solid phase is modeled constitutively; we address this aspect in the next section. The second has to do with the dimensionality of our simulations. Our simulations are 2D (a choice often found in the literature, in our case dictated by our computational resources, the real-time duration of each simulation and the number of simulations that our analysis requires). In actual fluidized beds the lateral motion of the solid has, we might say, two degrees of freedom (bubble-induced particle lateral motion develops in a horizontal plane), while in 2D fluidized beds only one degree of freedom is present (particle lateral motion can only develop along a horizontal line). Hence, when comparing lateral solid dispersion coefficients obtained numerically by means of 2D simulations with those estimated using empirical correlations, one needs to account for the 2D nature of the simulations. As discussed by Norouzi et al. (2011), omitting one dimension in the simulations significantly affects the value of the coefficient. The latter, in particular, is overestimated, as we have also observed in our work. We shall address this aspect in Section 5.2.

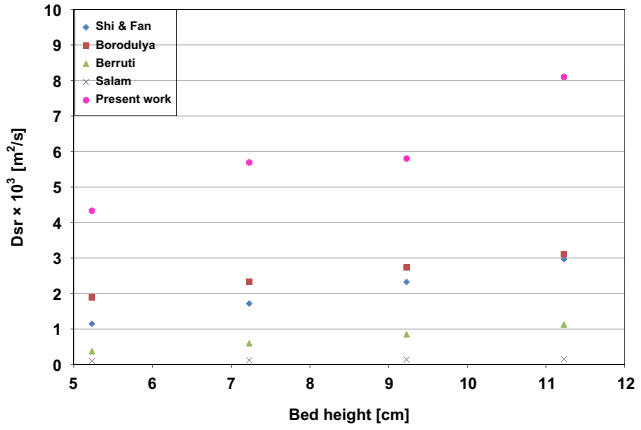

Fig. 5. Dispersion coefficient values at different minimum fluidization bed heights. The superficial fluid velocity is 1.07 m/s, while the bed width is 0.60 m. The values are compared with those obtained from empirical correlations in the literature.

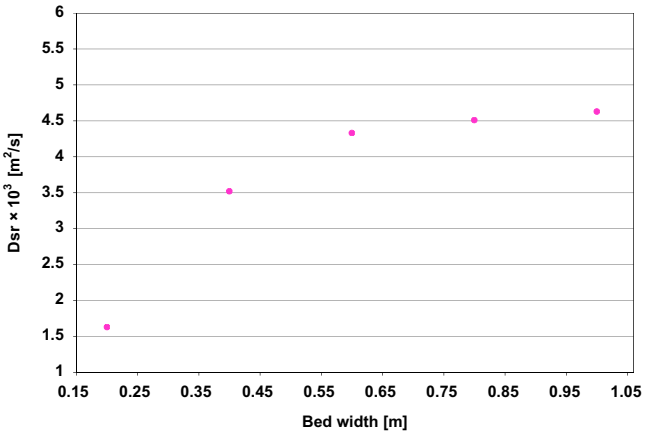

Fig. 7. Dispersion coefficient values at different bed widths. The superficial fluid velocity is 1.07 m/s, while the minimum fluidization bed height is 5.23 cm.

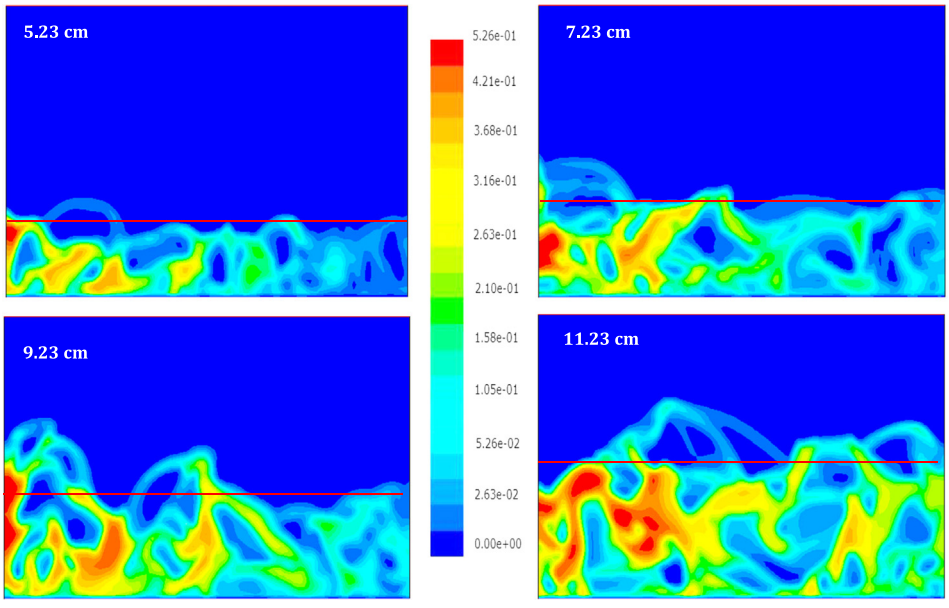

Fig. 6. Solid 1 volume fraction profiles at minimum fluidization bed heights of 5.23 cm, 7.23 cm, 9.23 cm and 11.23 cm. The superficial fluid velocity is 1.07 m/s, while the bed width is 0.60 m. The horizontal dashed line indicates where the bed ends and the freeboard begins.

5.1. Influence of hydrodynamic models

The Eulerian equations of motion adopted in this work, as said in Section 3, contain indeterminate terms that need to be expressed constitutively. Such terms are the fluid-particle and particle-particle interaction forces and the fluid and solid stress tensors. To close the stress tensors, one usually regards the phases as Newtonian continua; therefore, the closure relationships take the form reported in Eq. (17). So, the problem of closure reduces to finding constitutive expressions for the pressure, viscosity and dilatational viscosity for each phase. For the solid phases one needs to model these parameters constitutively.

To model the solid stress, one usually adopts the kinetic theory of granular flows (KTGF). This assumes that particles are smooth and spherical, that collisions are binary and instantaneous and that the powder is far from the frictional packing limit. Thus, the kinetic and collisional momentum transfer arising from the particle velocity fluctuations and the particle collisions are modeled following the Enskog theory for dense gases (Chapman and Cowling, 1970). Nevertheless, in several fluidized bed applications, like the one investigated in this work, particles interact largely through frictional enduring contacts, and the kinetic theory of granular flows does not take into account these important interactions. Hence, using the kinetic theory to model the solid stress in dense systems is inadequate and creates problems. We will now discuss in detail these problems.

In regions of high solid volume fraction, particles interact with multiple neighbors and the mechanism for stress generation is not just due to kinetic and (particularly) collisional contributions, but also to sustained contacts among particles. These contacts make particles dissipate a lot of energy, making them form very dense regions in the bed. This increases the ability of the granular assembly to resist shearing, because tangential frictional forces at contact points are now present. Consequently, the frictional viscosity of the bed is larger than that predicted by the granular kinetic theory model, insofar as this does not account for frictional interactions. So, using the kinetic theory alone to model dense fluidized beds underpredicts the solid viscosity, overestimating in turn the extent of particle mixing.

Enduring particle contacts in dense regions of fluidized beds do not only affect the viscosity of the solid phase, but also its pressure. The latter has a more pronounced effect on the fluid dynamics of the bed than the former, for the solid pressure influences significantly the formation and the size of the bubbles. Let us explain why. The two-phase theory by Toomey and Johnstone (1952) suggests that the void fraction around the bubbles and that in the emulsion phase are equal, for the theory assumes that all the gas in excess of that required to just fluidize the bed results in the formation of bubbles, the emulsion phase remaining at minimum fluidization conditions with uniform void fraction. However, local measurements of bed porosity by Lockett and Harrison (1967), done via capacitance probes, revealed that the void fraction around the bubbles is not uniform. This was observed experimentally by many other authors (Nguyen et al., 1973; Collins, 1989; Fan et al., 1990). Experimental investigations of voidage distributions around bubbles by Yates et al. (1994), and numerical simulations by Patil et al., (2005a), confirmed this, showing that the void fraction decreases exponentially from the bubble interface to the bulk of the emulsion phase. Fig. 8 reports the void fraction distribution around a bubble, as revealed by experimental and numerical studies (Patil et al., 2005b); regions A, B and C represent the bubble, the bubble boundary and the bulk of the emulsion phase, respectively. A question that one may want to ask is how the void fraction distribution around the bubbles and the frictional interactions among the particles affect the size of the bubbles. Answering this question will allow us to highlight the role of frictional stress on the dynamics of bubbling beds.

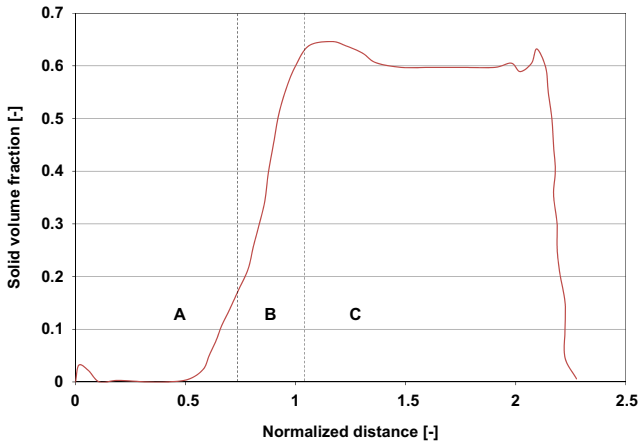

Fig. 8. Solid volume fraction profile vs. normalized distance from the bubble center (d_i/D_b), d_i is the distance from bubble center and D_b is the bubble diameter.

The bubble size is affected by the resistance that the gas finds to cross the bubble boundary and reach the emulsion phase. The larger the resistance, the less leaky the bubble boundary is and, in consequence, the larger the bubble results. The resistance through the bubble boundary depends on the drag experienced by the gas. This decreases when the void fraction around the bubbles increases. The frictional solid pressure strongly influences the void fraction distribution around the bubbles by reducing the compaction of solids around their interface, which increases the gas flow through the bubble boundary into the emulsion phase, thereby leading to smaller bubbles. Hence, if one employs the kinetic theory to model the solid pressure, without accounting for frictional stress, the solid pressure and in turn the void fraction around the bubbles are underestimated. This increases the drag experienced by the gas around the bubble boundaries and in turn reduces the gas leakage from the latter. This makes numerical simulations overestimate the sizes of the bubbles and the extent of particle mixing.

To overcome this problem, Johnson and Jackson (1987) proposed that the frictional stress should be added to the viscous stress modeled by the granular kinetic theory. The latter, as said, captures the flow regime in which the solid pressure is dictated mainly by kinetic and collisional contributions, whilst the former captures the flow regime in which enduring contacts are present among the particles. Even if the physical basis of adding the two stress contributions might be argued, the approach captures well the two extremes of granular flow. The frictional stress is usually modeled as follows:

$$\boldsymbol{\sigma_i^f} = p_i^f \boldsymbol{I} + \mu_i^f \left(\nabla \boldsymbol{u_i} + \nabla \boldsymbol{u_i}^T\right) \tag{28}$$

where p_i^f is the frictional pressure and μ_i^f is the frictional viscosity (the dilatational viscosity is usually neglected). When the solid volume fraction exceeds a threshold value ϕ_{min}, the frictional contribution to the solid pressure and viscosity are added to the viscous contribution:

$$p_i = p_i^v + p_i^f \quad ; \quad \mu_i = \mu_i^v + \mu_i^f \tag{29}$$

Johnson and Jackson (1987) proposed the following constitutive equation for the frictional pressure:

$$p_i^f = \begin{cases} F\frac{(\phi-\phi_{min})^a}{(\phi_{max}-\phi)^b}, & \phi \geq \phi_{min} \\ 0 & \phi < \phi_{min} \end{cases} \tag{30}$$

Here F, a and b are empirical constants, ϕ_{min} is the minimum solid volume fraction at which particles start generating stress through enduring contacts, while ϕ_{max} is the maximum volume fraction that the particles can attain. The frictional viscosity is then related

to the frictional pressure by the Coulomb (1776) friction law:

$$\mu_i^f = p_i^f \sin\varphi \tag{31}$$

where φ is the angle of internal friction of the granular material.

Another approach to modeling frictional stress was proposed by Shaeffer (1987) based on the principles of soil mechanics. The model reads:

$$p_i^f = 10^{25}(\phi - \phi_{min})^{10} \quad ; \quad \mu_i^f = \frac{p_i^f \sin\varphi}{2\sqrt{I_2}} \tag{32}$$

where I_2 is the second invariant of the deviatoric stress tensor.

Following the reasoning of Johnson and Jackson (1987), Srivastava and Sundaresan (2003) employed an additive approach to describe the solid stress, using Eq. (30) to model the frictional pressure. To model the frictional viscosity, they adopted a modified form of Shaeffer's model:

$$\mu_i^f = \frac{p_i^f \sin\varphi}{2\sqrt{I_2 + (\Theta_i/{d_p}^2)}} \tag{33}$$

where $\Theta_i$is the granular temperature and d_p is the particle diameter. The additional term $\Theta_i/{d_p}^2$ ensures that numerical singularity is avoided in regions where I_2 approaches zero, provided that in such regions the granular temperature does not vanish. They used this hybrid model to simulate the rise of a bubble in a fluid bed. To highlight the role of frictional stress on the bed dynamics, they ran another simulation without accounting for it. The results of their simulations revealed that frictional stress influences the bed dynamics significantly, affecting the shape and size of the bubbles.

Passalacqua and Marmo (2009) employed the model of Srivastava and Sundaresan (2003) to investigate the influence of frictional stress on bubble growth in fluidized beds. They reported that it affects significantly the size of the bubbles: with frictional stress accounted for, the predicted bubble size was significantly lower than that observed in simulations with no frictional stress implemented. They also showed that the value ascribed to ϕ_{min}, appearing in Eq. (30), plays a key role: the size of the bubbles predicted with lower values of ϕ_{min} are smaller than those obtained with higher values of the parameter. This is expected, for the lower the value of ϕ_{min}, the sooner frictional stress is accounted for (in the simulations) and the more particle compaction reduces around the bubbles; this in turn makes the latter leakier, reducing their sizes. This effect, as we shall see, affects significantly lateral dispersion.

In light of this, we conclude that the way in which frictional stress is modeled affects significantly the fluid dynamic behavior of fluidized beds; particularly in bubbling beds, where the latter is dictated mainly by the action of bubbles. In this section, we intend to investigate the role of frictional stress modeling on lateral solid mixing. These significantly influence bubble size and shape, which in turn affect how quickly the solid spreads throughout the bed. To investigate this aspect, we ran simulations using the operational conditions reported in Table 1 and considering the different cases outlined in Table 2. We tested different frictional pressure and viscosity models, changing the solid volume fraction at which the bed enters the frictional flow regime (ϕ_{min}) and observing the effects of these variations on lateral dispersion.

Fig. 9A shows the plot of the lateral dispersion coefficient against the superficial gas velocity for Cases 1 and 2. These cases are identical, except that in Case 2 frictional stress is introduced earlier (the value chosen for ϕ_{min} is lower). Fig. 9A shows that D_{sr} is predicted better in Case 2, its values being lower and closer to those found empirically. The same is observed for Cases 3 and 4, which are also identical, except that in Case 4 frictional stress is introduced earlier. Fig. 9B shows that the values of D_{sr} in Case 4 are lower than those in Case 3. This is because frictional stress is

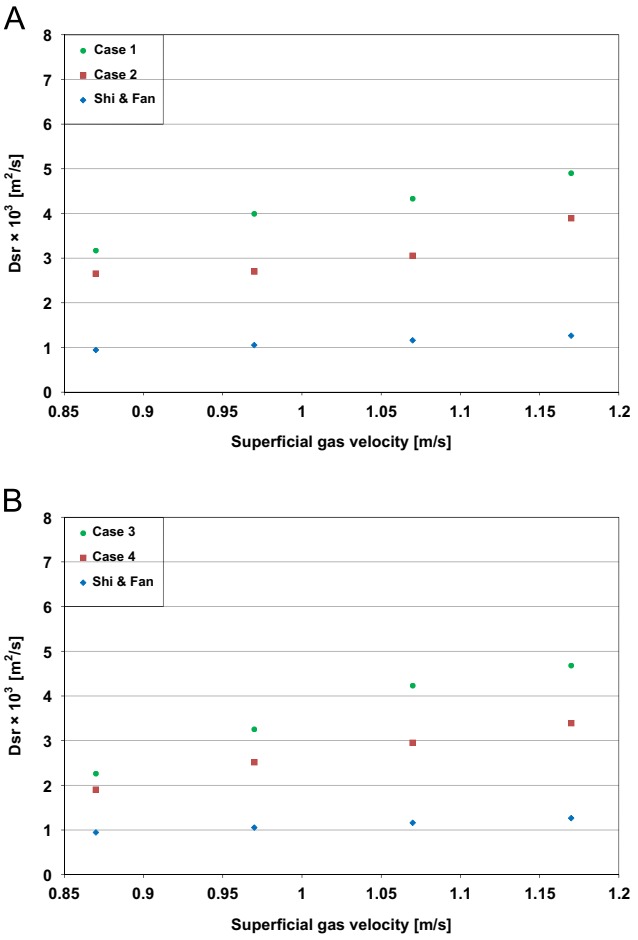

Fig. 9. Dispersion coefficient values at different superficial fluid velocities for different simulation cases. (A) Cases 1 and 2. (B) Cases 3 and 4. The minimum fluidization bed height is 5.23 cm, while the bed width is 0.60 m. The details of the cases are reported in Table 2.

introduced earlier. The effect of this, as said in the preceding paragraphs, is that the voidage around the bubbles increases, reducing the compaction of the particles and lowering the drag experienced by the fluid. Consequently, the leakage of gas through the bubble boundary increases, leading to bubbles of smaller size compared with cases where the introduction of the frictional stress is delayed. To illustrate this, we determined a statistical distribution of the bubble diameters by dividing the diameter range into classes, as shown in Fig. 10. Although there is no general consensus on how the equivalent bubble diameter should be defined, we took it to be the diameter of a circle having the same area (we are working in two dimensions) as the bubble. Thus, the equivalent bubble diameter is calculated as follows:

$$D_{eq} = \sqrt{\frac{4A}{\pi}} \tag{34}$$

where A denotes the area of the bubble. We used image analysis software to process the simulation results and compute the area of the bubbles. To do this, we assumed that bubbles are continuous regions in which the void fraction is larger than 0.85. By establishing a color contrast between these regions and the other parts of the bed, the software allows to determine the number of bubbles and their areas. Fig. 10 shows that Case 2, in which we introduced the action of frictional stress earlier, predicts the largest percentage of small-sized bubbles, which belong to diameter classes [0 cm, 1 cm] and [1 cm, 2 cm]. Conversely, Case 1 predicts higher percentages for greater bubble diameter classes. The reduction in

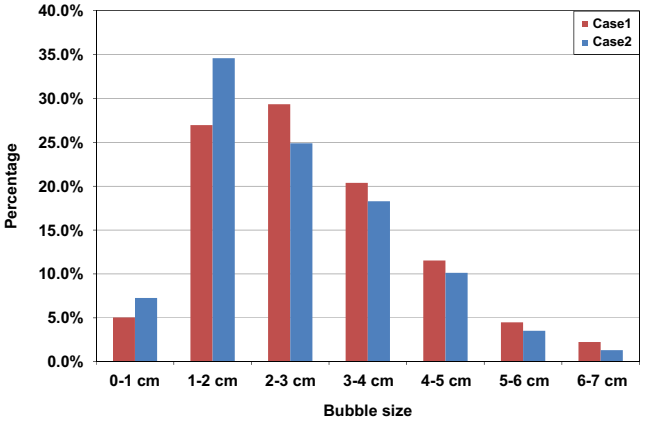

Fig. 10. Comparison of bubble size distributions for Cases 1 and 2. The superficial fluid velocity is 1.07 m/s, the minimum fluidization bed height is 5.23 cm, while the bed width is 0.60 m. The details of the cases are reported in Table 2.

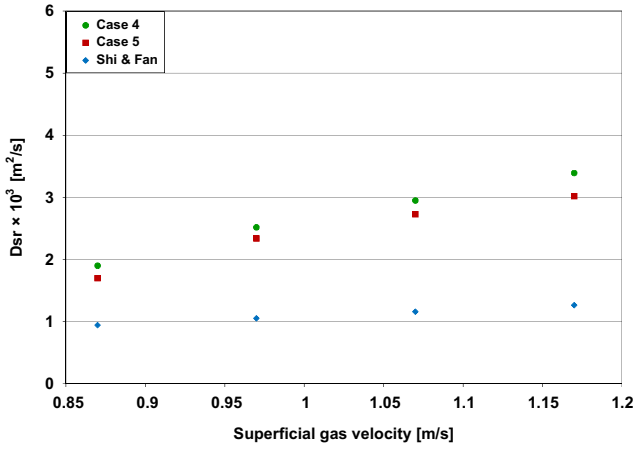

Fig. 11. Dispersion coefficient values at different superficial fluid velocities for Cases 4 and 5. The minimum fluidization bed height is 5.23 cm, while the bed width is 0.60 m. The details of the cases are reported in Table 2.

bubble size observed in Case 2 reduces the extent of lateral mixing, causing D_{sr} to have lower values.

To investigate the effects of frictional viscosity models on particle mixing, we compare Cases 1 and 3. In the first we adopted the model of Schaeffer (1987), while in the second that of Johnson and Jackson (1987). In both we used the same value for ϕ_{min}. As Figs. 9A and 9B show, Case 3 gives lower values for D_{sr}. This is because the model of Johnson and Jackson (1987) gives larger values of the frictional viscosity than those predicted by the model of Schaeffer (1987) (we verified this numerically). The larger the solid viscosity is, the more the granular assembly is able to resist shearing; this effect reduces the extent to which particles mix laterally, leading to lower values of the dispersion coefficient.

In the cases investigated, we highlighted the influence of frictional viscosity on lateral mixing, modeling the frictional pressure by means of the kinetic theory while varying the frictional viscosity model and the frictional packing limit. The simulation results revealed that increasing the effective viscosity of the solid slows down the bed dynamics, making the particles less able to mix, thereby reducing D_{sr}. We think that we can further improve the simulation results by changing the frictional pressure model. Thus, instead of modeling the frictional pressure using the kinetic theory, we used the semi-empirical model proposed by Johnson and Jackson (1987). The simulation set-up is shown in Table 2, Case 5. In Fig. 11 we compare the results obtained from Cases 4 and 5. In the latter we obtained lower D_{sr} values than in the former for all values of the superficial gas velocity. This is expected because the frictional pressure predicted by the model of Johnson & Jackson, used in Case 5, is higher than that predicted by the kinetic theory model, used in Case 4 (for a quantitative comparison between these pressure models, we refer to Passalacqua and Marmo, 2009). The higher frictional pressure is, the higher the void fraction around bubbles is, and the leakier the latter become. Consequently, Case 5 predicts smaller bubbles than Case 4. To confirm this, we carried out a statistical analysis of the bubble size distributions on these cases, as we did previously. This is reported in Fig. 12. We observe that Case 5 has a higher proportion of small bubbles in the size range [0, 1 cm], [1 cm, 2 cm] and [2 cm, 3 cm].

The results obtained revealed that Case 5 gives the best set-up for predicting D_{sr}. To confirm this, we used the set-up in Case 5 to investigate Powder 2. The properties of this powder are reported in Table 3. We compared the results with those obtained using the set-up in Case 1 (which is the default in Fluent). We began by investigating the influence of the superficial gas velocity on the dispersion coefficient. To do this, we kept the minimum

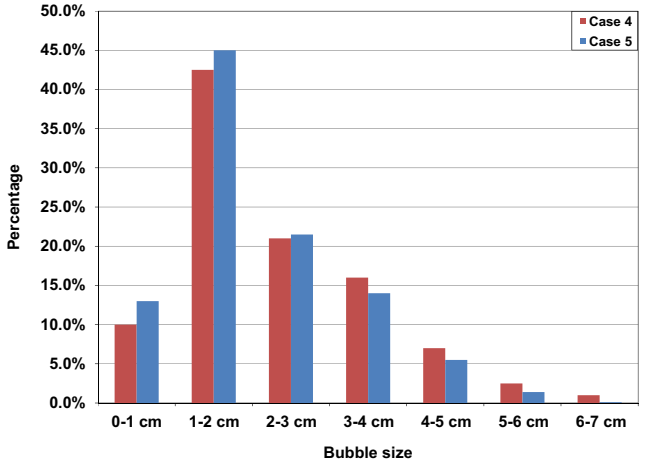

Fig. 12. Comparison of bubble size distributions for Cases 4 and 5. The superficial fluid velocity is 1.07 m/s, the minimum fluidization bed height is 5.23 cm, while the bed width is 0.60 m. The details of the cases are reported in Table 2.

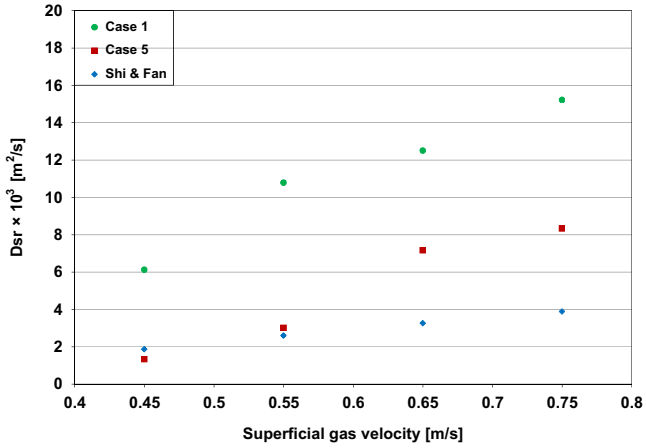

Fig. 13. Dispersion coefficient values at different superficial fluid velocities for Cases 1 and 5 for Powder 2. The minimum fluidization bed height is 17.0 cm, while the bed width is 0.90 m. The details of the cases are reported in Table 2.

fluidization bed height at 0.17 m and the bed width at 0.9 m, we fluidized the bed at different superficial gas velocities and we calculated the values of the dispersion coefficient. The results are

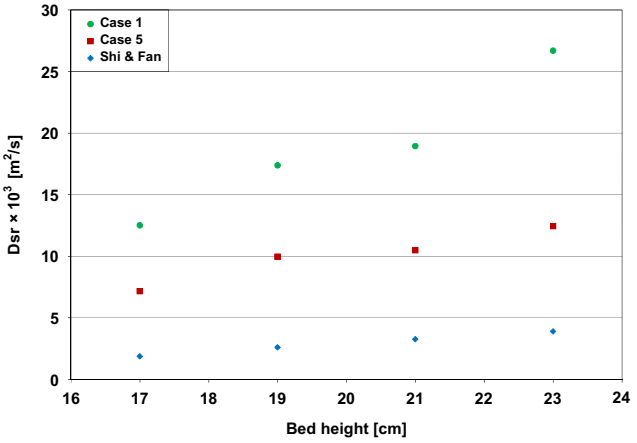

Fig. 14. Dispersion coefficient values at different minimum fluidization bed heights for Cases 1 and 5 for Powder 2. The superficial fluid velocity is 0.65 m/s, while the bed width is 0.90 m. The details of the cases are reported in Table 2.

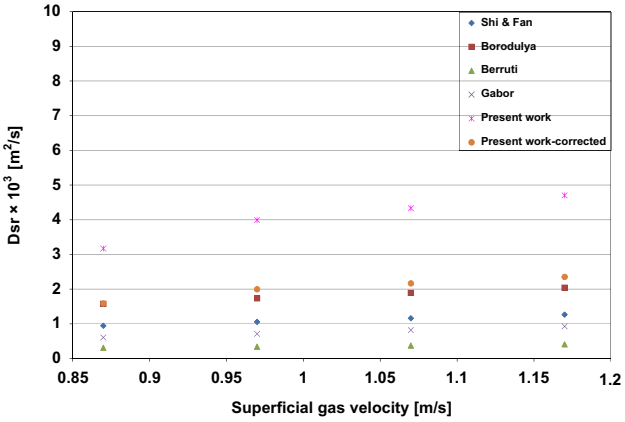

Fig. 15. Comparison of dispersion coefficient values obtained by scaling down the original results in Case 1. The details of the cases are reported in Table 2. The values are compared with those obtained from empirical correlations in the literature.

reported in Fig. 13. The trends observed are similar to what we reported for Powder 1: the dispersion coefficient increases with the superficial gas velocity, and Case 5 gives better predictions than Case 1. We also ran simulations changing the bed height and keeping the superficial gas velocity and bed width at 0.65 m/s (2.6 times u_{mf}) and 0.9 m, respectively. Fig. 14 shows that the dispersion coefficient increases with bed height, and that Case 5 predicts better results than Case 1.

5.2. Effect of simulation dimensionality

As mentioned in the general discussion, the overestimation of D_{sr} is partly due to the 2D nature of our simulations, which reduces the degrees of freedom of lateral solid motion. To assess how the dimensionality of our simulations affects the numerical results, we scaled down the numerical values obtained for D_{sr} by a factor α, to account for the dimensionality difference between the 2D domain used in our simulations and the 3D nature of the fluidized beds to which the empirical correlations used for validation refer. So, the dispersion coefficient values found empirically were no longer compared with the values D_{sr} found numerically, but rather with the scaled values D_{sr}/α. To a first approximation, it was speculatively assumed that scaling could be accomplished by accounting for the degree of freedom lost when passing from a 3D to a 2D case, hence $\alpha = 2$. Fig. 15 reports, for Case 1, the original and scaled-down values of the dispersion coefficient obtained numerically and those obtained from the empirical correlations. The scaled values of D_{sr} compare fairly well with predictions of Borodulya et al. (1982), but are still larger than the values yielded by the other empirical correlations. Altogether, it may be concluded that values of D_{sr} of reasonable accuracy can be obtained from 2D simulations with proper consideration of particle frictional stress combined with scaling to account for simulation dimensionality.

6. Conclusions

In this work we investigated lateral solid mixing in fluidized beds using a Eulerian-Eulerian modeling approach. We defined the lateral dispersion coefficient D_{sr} using an equation analogous to the Fick's law of molecular diffusion. We examined the influence of design parameters and operational conditions on the values of D_{sr}, considering how the latter is affected by the constitutive equations used to model the frictional solid stress. The simulation results show that D_{sr} increases with the superficial gas velocity and bed height. We also observed that D_{sr} increases rapidly at low values of bed width, but as this increases, D_{sr} rises slowly and then remains approximately constant. Furthermore, we investigated the influence of the fluid-dynamic model used in the simulations on the numerical results. To do so, we ran simulations with different frictional pressure and viscosity models, changing the solid volume fraction at which the bed is assumed to enter the frictional flow regime. The results showed that the model choice significantly affects the numerical results. Bubble size distributions in the bed show that early introduction of frictional solid stress results in the formation of smaller bubbles, leading to lower values of D_{sr}. We confirmed such findings by running simulations with another powder. For the two sets of powders, we obtained similar trends in D_{sr} values. Finally, we examined the influence that the 2D dimensionality of our simulations has on the numerical results obtained. The overestimation found is partly due to this dimensionality issue. A simple scaling rule based on the consideration of the loss of degree of freedom of lateral particle motion when passing from a 3D to a 2D domain was effective to largely reconcile simulated and empirical values of D_{sr}.

References

Avidan, A., Yerushalmi, J., 1985. Solids mixing in an expanded top fluid bed. AIChE J. 31, 835–841.
Bellgardt, D., Schoessler, M.,, Werther, J.,, 1987. Lateral nonuniformities of solids and gas concentrations in fluidized bed reactors. Powder Technol. 53, 205–216.
Berruti, F., Scott, D.S., Rhodes, E., 1986. Measuring and modelling lateral solid mixing in a three dimensional batch gas-solid fluidized bed reactor. Can. J. Chem. Eng. 64, 48–56.
Borodulya, V.A., Epanov, Y.G., Teplitskii, Y.S., 1982. Horizontal particle mixing in a free fluidized bed. J. Eng. Phys. 42, 528–533.
Brotz, W., 1956. Untersuchungen über Transportvorgänge in durchströmtem, gekömtem Gut. Chem. Ing. Tech. 28, 165–174.
Carstensen, J.T., Patel, M.R., 1977. Blending of irregularly shaped particles. Powder Technol. 17, 273–282.
Chapman, S., Cowling, T.G., 1970. *The Mathematical Theory of Non-Uniform Gases*. Cambridge University Press.
Collins, R., 1989. A model for the effects of the voidage distribution around a fluidization bubble. Chem. Eng. Sci. 44, 1481–1487.
Coroneo, M., Mazzei, L., Lettieri, P., Paglianti, A., Montante, G.,, 2011. CFD prediction of segregating fluidized bidisperse mixtures of particles differing in size and density in gas-solid fluidized beds. Chem. Eng. Sci. 66, 2317–2327.
Coulomb, C.A., 1776. Essai sur une application des règles de maximis et minimis à quelques problèmes de statique, relatifs à l'architecture. Acad. Roy. Des Sci. 7, 343–382.
Du, B., Fan, L.-S., Wei, F., Warsito, W., 2002. Gas and solids mixing in a turbulent fluidized bed. AIChE J. 48, 1896–1909.
Fan, Z., Chen, G.T., Chen, B.C., Yuan, H., 1990. Analysis of pressure fluctuations in a 2-D fluidized bed. Powder Technol. 62, 139–145.

Farzaneh, M., Sasic, S., Almstedt, A., Johnsson, F., Pallarès, D., 2011. A novel multigrid technique for lagrangian modeling of fuel mixing in fluidized beds. Chem. Eng. Sci. 66, 5628–5637.
Gidaspow, D., 1994. Multiphase Flow and Fluidization. Academic Press, Boston.
Gómez-Barea, A., Leckner, B., 2010. Modeling of biomass gasification in fluidized bed. Prog. Energ. Combust. 36, 444–509.
Johnson, P.C., Jackson, R., 1987. Frictional-collisional constitutive relations for granular materials, with application to plane shearing. J. Fluid Mech. 176, 76–93.
Kashyap, M., Gidaspow, D., 2011. Measurement of dispersion coefficients for FCC particles in a free board. Ind. Eng. Chem. Res. 50 (12), 7549–7565.
Kunii, D.,, Levenspiel, O., 1989. Fluidization Eng.. Butterworth Heinemann.
Lebowitz, J.L., 1964. Exact solution of generalised Percus-Yevick equation for a mixture of hard spheres. Phys. Rev. 133, 895–899.
Lacey, P.M.C., 1954. Developments in theory of particle mixing. J. Appl. Chem, 257–268.
Lettieri, P., Mazzei, L., 2009. Challenges and issues on the CFD modeling of fluidized beds: a review. J. Comput. Multiphase Flow 1, 83–131.
Lewis, W.K., Gilliland, E.R., Girouard, H., 1962. Heat transfer and solids mixing in a bed of fluidized solids. Chem. Eng. Prog. Symp. 58, 87–97.
Liu, D., Chen, X., 2010. Lateral solid dispersion in large scale fluidized beds. Combust. Flame 157, 2116–2124.
Lun, C.K.K., Savage, S.B., Jerey, D.J., Chepurniy, N., 1984. Kinetic theories for granular flow: inelastic particles in Couette flow and slightly inelastic particles in a general flow field. J. Fluid Mech. 140, 223–256.
May, W.G., 1956. Fluidized bed reactor studies. Chem. Eng. Prog. 55, 49–56.
Mazzei, L.,, 2013. Segregation dynamics of dense polydisperse fluidized suspensions modeled using a novel formulation of the direct quadrature method of moments. Chem. Eng. Sci. 101, 565–576.
Mazzei, L.,, 2011. Limitations of quadrature-based moment methods for modeling inhomogeneous polydisperse fluidized powders. Chem. Eng. Sci. 66, 3628–3640.
Mazzei, L., Lettieri, P., 2007. A drag force closure for uniformly-dispersed fluidized suspensions. Chem. Eng. Sci. 62, 6129–6142.
Mazzei, L., Lettieri, P.,, 2008. CFD simulations of expanding/contracting homogeneous fluidized beds and their transition to bubbling. Chem. Eng. Sci. 63, 5831–5847.
Mazzei, L., Casillo, A., Lettieri, P., Salatino, P., 2010. CFD simulations of segregating fluidized binary mixtures of particles differing in size. Chem. Eng. J. 156, 432–445.
Mostoufi, N., Chaouki, J., 2001. Local solid mixing in gas-solid fluidized beds. Powder Technol. 114, 23–31.
Norouzi, H.R., Mostoufi, N., Mansourpour, Z., Sotudeh-Gharebagh, R., Chaouki, J., 2011. Characterization of solids mixing patterns in bubbling fluidized beds. Chem. Eng. Res. Design 89, 817–826.
Nguyen, X.T., Leung, L.S., Weiland, R.H., 1973. On void fractions around a bubble in a two-dimensional fluidized bed (Proceedings of the International Congress on Fluidization and its Applications). In: Angelino, H., Couderc, J.P., Gilbert, H., Laguerie, C. (Eds.), Societe de Chemie Industrielle, Paris, pp. 230–239 (Toulouse).
Owoyemi, O., Mazzei, L., Lettieri, P., 2007. CFD modeling of binary-fluidized suspensions and investigation of role of particle-particle drag on mixing and segregation. AIChE J. 53, 1924–1940.
Passalacqua, A., Marmo, L., 2009. A critical comparison of frictional stress models applied to the simulation of bubbling fluidized beds. Chem. Eng. Sci. 160, 2795–2806.
Patil, D.J., van Sint Annaland, M., Kuipers, J.A.M., 2005a. Critical comparison of hydrodynamic models for gas-solid fluidized beds – part I: bubbling gas-solid fluidized beds operated with a jet. Chem. Eng. Sci. 60, 57–72.
Patil, D.J., van Sint Annaland, M., Kuipers, J.A.M., 2005b. Critical comparison of hydrodynamic models for gas-solid fluidized beds – part II: freely bubbling gas-solid fluidized beds. Chem. Eng. Sci. 60, 73–84.
Rhodes, M., Zhou, S., Hirama, T., Cheng, H., 1991. Effects of operating conditions on longitudinal solids mixing in a circulating fluidized bed riser. AIChE J. 37, 1450–1458.
Salam, T.F., Ren, Y., Gibbs, B.M., 1987. Lateral solid and thermal dispersion in fluidized bed combustors. Proc. Int. Conf. Fluid Bed Combust. 9, 541.
Schaeffer, D.G., 1987. Instability in evolutions describing incompressible granular flow. J. Differ. Equations 66, 19–50.
Shi, Y., Fan, L.T., 1984. Lateral mixing of solids in batch gas-solid fluidized beds. Ind. Eng. Chem. Process Design Dev. 1084 (23), 337–341.
Srivastava, A., Sundaresan, S., 2003. Analysis of a frictional–kinetic model for gas–particle flow. Powder Technol. 129, 72–85.
Syamlal, M., Rogers, W.A., O'Brien, T.J., 1993. MFIX documentation and theory guide, DOE/METC94/1004, NTIS/DE94000087. ⟨http://www.mfix.org⟩.
Tagliaferri, C., Mazzei, L., Lettieri, P., Marzocchella, A., Olivieri, G., Salatino, P.,, 2013. CFD simulation of bubbling fluidized bidisperse mixtures: Effect of integration methods and restitution coefficient. Chem. Eng. Sci. 102, 324–334.
Toomey, R.D., Johnstone, H.F., 1952. Gaseous fluidization of solid particles. Chem. Eng. Prog. 48, 220–226.
Winaya, I.N.S., Shimizu, T., Yamada, D., 2007. A new method to evaluate horizontal solid dispersion coefficient in a bubbling fluidized bed. Powder Technol. 178, 173–178.
Xiang, Q., Huang, G., Ni, M., Cen, K., Tao, T., 1987. Lateral dispersion of large coal particles in an industrial-scale fluidized. Proc. Int. Conf. Fluid Bed Combust. 9, 546.